Published for SISSA by Springer

Received: March 11, 2014
Revised: June 14, 2014
Accepted: June 30, 2014
Published: July 28, 2014

On the ratio of $t\bar{t}b\bar{b}$ and $t\bar{t}jj$ cross sections at the CERN Large Hadron Collider

G. Bevilacqua[a] **and M. Worek**[b]

[a] *INFN, Laboratori Nazionali di Frascati, Via E. Fermi 40, I-00044 Frascati, Italy*

[b] *Institute for Theoretical Particle Physics and Cosmology, RWTH Aachen University, Otto-Blumenthal Str., D-52056 Aachen, Germany*

E-mail: Giuseppe.Bevilacqua@lnf.infn.it, worek@physik.rwth-aachen.de

Abstract: Triggered by ongoing experimental analyses, we report on a study of the cross section ratio $\sigma(pp \to t\bar{t}b\bar{b})/\sigma(pp \to t\bar{t}jj)$ at the next-to-leading order in QCD, focusing on both present and future collider energies: $\sqrt{s} = 7$, 8, 13 TeV. In particular, we provide a comparison between our predictions and the currently available CMS data for the 8 TeV run. We further analyse the kinematics and scale uncertainties of the two processes for a single set of parton distribution functions, with the goal of assessing possible correlations that might help to reduce the theoretical error of the ratio and thus enhance the predictive power of this observable. We argue that the different jet kinematics makes the $t\bar{t}b\bar{b}$ and $t\bar{t}jj$ processes uncorrelated in several observables, and show that the scale uncertainty is not significantly reduced when taking the ratio of the cross sections.

Keywords: QCD Phenomenology, NLO Computations

ArXiv ePrint: 1403.2046

doi:10.1007/JHEP07(2014)135

JHEP07(2014)135

Contents

JHEP07(2014)135

1 Introduction

In order to establish whether the scalar resonance observed at the Large Hadron Collider (LHC) around 125 GeV [1, 2] matches the properties of the Standard Model (SM) Higgs boson, quantities such as the couplings to fermions have to be measured with high precision. A special interest is due to the Yukawa couplings to top (Y_t) and bottom (Y_b) quarks. Massive as they are, these quarks are ideal candidates for probing the nature of the new particle and more generally of the Electroweak Symmetry Breaking mechanism.

For a SM Higgs boson with the observed mass value, the dominant decay mode is $H \to b\bar{b}$ [3]. The presence of an overwhelming QCD background discourages Higgs searches in the direct production channel $pp \to H \to b\bar{b}$. Attention is rather put on Higgs production in association with one or more additional objects [4–7] due to the fact that backgrounds are easier to control in such an environment.

Among all the associated production mechanisms that have been explored by the ATLAS and CMS Collaborations, the $pp \to t\bar{t}H \to t\bar{t}b\bar{b}$ channel plays an important role [8–10]. The production rate for this process is directly sensitive to $\sim (Y_t^2\, Y_b^2)/\Gamma_H$, where Y_t and Y_b are the top- and the bottom-Yukawa coupling respectively and Γ_H is the Higgs boson width (see figure 1, diagram A). Since the total Higgs boson width can be constrained via independent measurements, e.g. by the ratio of off-shell and on-shell production and decay rates in the $H \to ZZ \to 4\ell$ and/or the $H \to W^+W^- \to 2\ell\, 2\nu$ channel [11–14], the $t\bar{t}H \to t\bar{t}b\bar{b}$ process adds to the information on Y_b provided by $pp \to VH(H \to b\bar{b})$, where $V = Z/W^{\pm}$.

However, the $t\bar{t}H(H \to b\bar{b})$ final state is very challenging to measure. Search strategies employed by both experiments are based on the full reconstruction of the $t\bar{t}b\bar{b}$ final state

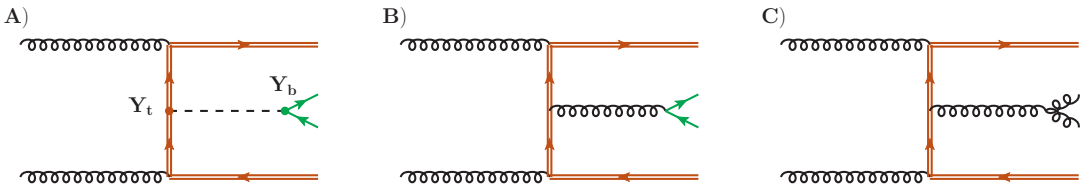

Figure 1. Representative Feynman diagram for the associated production of the Higgs boson and a $t\bar{t}$ pair followed by the decay of the Higgs boson into a $b\bar{b}$ pair (diagram A). Also shown are representative Feynman diagrams for the irreducible background with the same final state (diagram B), as well as the reducible background with two jets (diagram C). A single dashed line corresponds to the Higgs boson, double lines correspond to top quarks, single lines to bottom quarks and wiggly ones to gluons.

from charged leptons, missing energy and jets [15–18]. Using b-jet tagging, events with four b-jets are isolated, and the decays of the two candidate top quarks are reconstructed. Afterwards, the two b-jets which have not been associated to top decays are assigned to the candidate Higgs boson's decay. It should be clear that the identification of such decay products is not free of ambiguities. The so-called combinatorial background is responsible for a substantial smearing of the Higgs boson peak in the $b\bar{b}$ invariant mass. Together with the possibility of misidentifying light jets with b-jets, this represents a serious obstacle to the observation of the Higgs signal and demands a good control of dominant backgrounds as a prerequisite for a successful analysis. Several strategies have been presented in the literature to increase a sensitivity for this challenging channel. The most promising being the jet substructure techniques for boosted heavy states and the matrix element methods [19–21] to name just a few examples.

The process of $t\bar{t}b\bar{b}$ production in QCD is the most important irreducible background for the signal under consideration (see figure 1, diagram B). With the help of b-jet tagging algorithms, it is possible to isolate the contribution of this process from the most general reducible background represented by $t\bar{t}jj$ production (see figure 1, diagram C). Instead of extracting absolute cross sections, one can measure the production rate of $t\bar{t}b\bar{b}$ normalized to the inclusive $t\bar{t}jj$ sample. This procedure has been explored by both CMS and ATLAS Collaborations [22–24] and has the advantage that many experimental systematics, including luminosity uncertainty, lepton identification and jet reconstruction efficiency, are expected to cancel in the ratio. The overall systematic error should thus be dominated by the efficient and clean identification of bottom jets, referred to as the b-jet tagging efficiency, as well as the tagging efficiency for the light flavor jets, referred to as the mistag rate.

On the theory side, the QCD backgrounds $pp(p\bar{p}) \to t\bar{t}b\bar{b}$ and $pp(p\bar{p}) \to t\bar{t}jj$ have been calculated at the next-to-leading order (NLO) in QCD [25–30]. Fairly moderate, $\mathcal{O}(15\% - 30\%)$ corrections have been found for both processes. The estimated theoretical uncertainties due to truncation of higher-order terms in the perturbative expansion are of the same size. In addition, first results for $t\bar{t}$ production in association with either two light or two bottom jets, and enhanced by a parton shower have recently appeared [31–33]. Scale variations before and after matching have been assessed to be rather similar. Each of these

JHEP07(2014)135

calculations, however, has been carried out with different sets of cuts, jet algorithms, values of top quark mass and parton distribution functions (PDFs). This makes a determination of the cross section ratio possible only at the price of introducing undesired additional theoretical uncertainties.

The purpose of this paper is twofold. First, we would like to provide a systematic analysis of $t\bar{t}b\bar{b}$ and $t\bar{t}jj$ backgrounds and extract the most accurate NLO predictions for the cross section ratio, to be used in comparisons with the available LHC data. The second goal is to examine whether the ratio has enhanced predictive power for Higgs searches, by investigating possible correlations between the two processes in the quest of reducing theoretical errors.

The paper is structured as follows. In section 2 we assess the kinematical range of our predictions, i.e. we motivate which phase space restrictions, particularly in the transverse momentum of jets, shall be applied for our fixed-order results to be reliable. Beyond these limits, the stability of the perturbative expansion is likely to be endangered, and resummation of higher order effects is required. We estimate these limits by studying leading-order $t\bar{t}jj$ production matched with Pythia parton shower, and use the obtained results to determine the kinematical setup for our predictions. In section 3 we examine next-to-leading order differential cross sections for both $t\bar{t}b\bar{b}$ and $t\bar{t}jj$ processes, analysing similarities and possible correlations between the two backgrounds. Subsequently, we provide in section 4 the results for the ratio and absolute cross sections for three different collider energies: $\sqrt{s} = 7$, 8 and 13 TeV. Section 5 is devoted to a comparison with the currently available CMS data at $\sqrt{s} = 8$ TeV. Finally, in section 6 we draw our conclusions.

2 Leading order results with parton shower

We begin our analysis by exploring the validity domain of our perturbative calculation. To this end, we have generated an inclusive parton-level sample of $pp \to t\bar{t}jj$ where j stands for u, d, c, s, b or g. The event sample has been produced with Helac-Phegas [34–36] in the Les Houches event file format [37] and interfaced with the general purpose Monte Carlo program Pythia 6.4 (version 6.427) [38] to include initial- and final-state shower effects. We simulate pp collisions at $\sqrt{s} = 8$ TeV using the following parton level cuts,

$$\begin{aligned} p_{T_j} &= \sqrt{p_{x_j}^2 + p_{y_j}^2} > 10 \text{ GeV}\,, \\ |y_j| &= \left|\frac{1}{2}\ln\left(\frac{E_j + p_{z_j}}{E_j - p_{z_j}}\right)\right| < 4.5\,, \\ \Delta R_{jj} &= \sqrt{\Delta\phi_{jj}^2 + \Delta y_{jj}^2} > 0.4\,, \end{aligned} \tag{2.1}$$

where p_{T_j}, y_j and ΔR_{jj} denote transverse momentum, rapidity and distance between the two jets in the (y, ϕ) plane respectively. The top quark mass is set to the value $m_t = 173.5$ GeV [39] and top quarks are assumed to be stable. All the other QCD partons, including bottom quarks, are treated as massless. We work within the 5-flavor scheme, taking a LO PDF set with a 1-loop running strong coupling constant and five active flavors, $N_F = 5$. More specifically, the Les Houches Accord PDF implementation [40–42] of the

JHEP07(2014)135

CT09MC1 PDF set [43] is used with the corresponding value of α_s evaluated for $\mu = m_t$. Jets are reconstructed out of the partonic final state emerging after shower, using the *anti-k_T* jet clustering algorithm [44] provided by the FastJet package [45, 46]. The jet cone size is set to $R = 0.5$, and reconstructed jets are required to satisfy

$$p_{T_j} > 20 \text{ GeV}, \qquad |y_j| < 2.5, \qquad \Delta R_{jj} > 0.5\,. \tag{2.2}$$

To allow for a more direct comparison with our fixed-order results, we decide to stop the evolution at the end of the perturbative phase. In other words, we neglect effects related to hadronization, underlying events or multiple pp interactions. Also, decays of the top quark and QED radiation from quarks are switched off. All the other Pythia parameters have been left unchanged and correspond to default settings.

We have considered two different variants of shower, both provided within Pythia 6.4: transverse-momentum ordered shower (dubbed Pythia$_{p_T}$) and virtuality-ordered or mass-ordered shower (dubbed Pythia$_{Q^2}$). The starting scale for the shower has been set to $p_{T_j}^{\min}$ and $m_{jj}^{\min} = p_{T_j}^{\min}\sqrt{2(1-\cos R)}$ respectively. As a consistency check, we have compared the total rate obtained after showering with the LO expectation based on our selection cuts. We obtain the following cross sections:

$$\begin{aligned}
\sigma_{pp\to t\bar{t}jj}^{\text{HELAC+PYTHIA}_{p_T}} &= 69.6 \text{ pb}\,,\\
\sigma_{pp\to t\bar{t}jj}^{\text{HELAC+PYTHIA}_{Q^2}} &= 63.7 \text{ pb}\,,\\
\sigma_{pp\to t\bar{t}jj}^{\text{HELAC-PHEGAS}} &= 77.1 \text{ pb}\,.
\end{aligned} \tag{2.3}$$

The two showered results, based on different shower ordering variables, agree within 9% and are comparable with the LO cross section.

In a subsequent step, we compare leading-order predictions at the differential level before and after showering. Figure 2 shows distributions of the transverse momentum of the two hardest jets, the dijet invariant mass and the transverse momentum of the $t\bar{t}j_1$ system, where j_1 denotes the first hardest jet. We observe that p_T and invariant mass distributions are not strongly modified by the parton shower. Shape differences are within the corresponding theoretical errors, that we did not report on the plots for better readability. On the other hand, the transverse momentum distribution of the $t\bar{t}j_1$ system shows a sizeable discrepancy in the low-p_T region. Note that at leading-order, momentum conservation sets the equality $p_T(t\bar{t}j_1) = p_T(j_2)$, where j_2 is the second hardest jet, and thus the distributions of these two observables coincide. When the parton shower is turned on, the extra radiation allows the presence of additional jets, and the direct relation between the previous two quantities is lost. A large Sudakov suppression is visible starting approximately below $p_{t\bar{t}j_1} = 40\,\text{GeV}$, while the fixed-order result displays a sharp peak.[1]

[1] Similar conclusions have been obtained before for example in case of $t\bar{t}j$ either by means of matching different LO multijet matrix elements with showering programs [47] or by matching the NLO $t\bar{t}j$ matrix element with parton shower via the Powheg method [48].

JHEP07(2014)135

This discrepancy indicates that dominant higher-order effects endanger the stability of the perturbative expansion in the small p_T region for this observable. Therefore to be on the safe side for all observables the following choice of basic selection cuts is taken for a reliable fixed-order analysis:

$$p_{T_j} > 40 \text{ GeV}, \qquad |y_j| < 2.5, \qquad \Delta R_{jj} > 0.5\,. \tag{2.4}$$

The specific value of the cut on the maximum jet rapidity is dictated by the detector acceptance and the experimental requirements for the bottom flavor jet reconstruction [49]. We report for completeness the total LO cross sections that we obtain using the cuts (2.4):

$$\begin{aligned}
\sigma_{pp\to t\bar{t}jj}^{\text{HELAC+PYTHIA}_{p_T}} &= 26.4 \text{ pb}\,,\\
\sigma_{pp\to t\bar{t}jj}^{\text{HELAC+PYTHIA}_{Q^2}} &= 23.1 \text{ pb}\,,\\
\sigma_{pp\to t\bar{t}jj}^{\text{HELAC-PHEGAS}} &= 28.1 \text{ pb}\,.
\end{aligned} \tag{2.5}$$

Let us conclude this section by saying that the main point here was to justify our choice of the p_T cut on the jets. We were not aiming at a very precise description of particular observables, such as the p_T of the $t\bar{t}j$ system, over the complete range of transverse momenta. For this reason, we made some approximations, which are, in our opinion, justified by our goal. These approximations consist of: lack of merging of samples with different multiplicity, lack of elimination of double counting. We stress that a more involved procedure without these approximations would not change our conclusion, which is that a lowest p_T of 40 GeV is very safe from the point of view of the reliability of the fixed order prediction. To be very precise, what mattered to us, was the point where a showered distribution diverges from the fixed order one. Merging, on the other hand, would mostly improve the low p_T range.

Let us also stress here, that we have drawn similar conclusions from matching the leading order $pp \to t\bar{t}b\bar{b}$ event sample with p_T-ordered and Q^2-ordered showers from PYTHIA. In that case, however, initial state configurations with a b-quark have been neglected in the leading order $pp \to t\bar{t}b\bar{b}$ event sample. Such contributions are usually neglected in calculations for final states involving a $b\bar{b}$ pair. The reason is simple: they contribute at the level of a percent, as has been checked in many studies in the past. In view of the quality of the prediction such contributions are irrelevant, but make the technical side of the work more involved. Of course, a shower will not change anything here.

3 Next-to-leading order differential cross sections

Having established a safe kinematical domain, we now turn to examine the behavior of differential cross sections for both processes, $pp \to t\bar{t}b\bar{b}$ and $pp \to t\bar{t}jj$, where j stands for u, d, c, s, b, g together with corresponding anti-quarks. Also here initial state configurations with a b-quark are neglected in calculations for the $pp \to t\bar{t}b\bar{b}$ final state. As already

JHEP07(2014)135

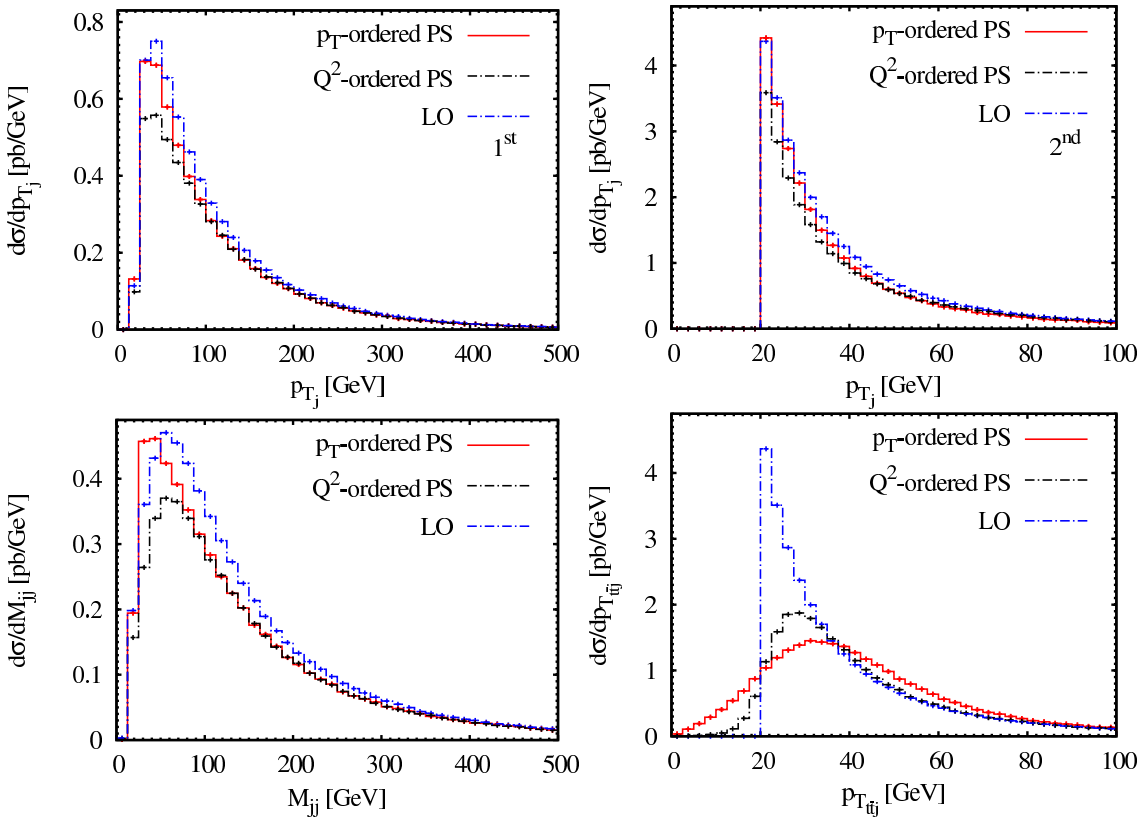

Figure 2. Comparison between the LO results obtained with HELAC-PHEGAS and the LO+LL results produced by matching LO predictions to PYTHIA for $pp \to t\bar{t}jj$ at the LHC with $\sqrt{s} = 8$ TeV. The dash-dotted (blue) curve corresponds to the LO whereas the solid (red) to the LO+LL based on transverse-momentum-ordered parton shower and the dashed (black) curves to the LO+LL with virtuality-ordered shower. The following distributions are shown: transverse momentum of the first and the second hardest jet (upper panel), invariant mass of the two hardest jets and transverse momentum of the $t\bar{t}j$ system (lower panel).

mentioned, we are interested in investigating similarities and correlations between the two backgrounds with the goal of reducing theoretical uncertainties in the cross section ratio.

Our NLO results are based on NLO CTEQ PDF set, i.e. CT10 [50], including 2 loop running of α_s and $N_F = 5$, with $\mu_R = \mu_F = \mu_0$ for the renormalization and factorization scales, where[2]

$$\mu_0^2(pp \to t\bar{t}b\bar{b}) = m_t \sqrt{\prod_{i=1}^{2} p_T(b_i)} \quad , \tag{3.1}$$

$$\mu_0^2(pp \to t\bar{t}jj) = m_t^2 \, . \tag{3.2}$$

Jets are reconstructed using the *anti-k_T* clustering algorithm with resolution parameter $R = 0.5$. We require the presence of at least two jets and impose the selection cuts of eq. (2.4). No restriction on the kinematics of the possible third jet is applied.

[2]This scale choice for the $pp \to t\bar{t}b\bar{b}$ process has been first introduced in ref. [27].

JHEP07(2014)135

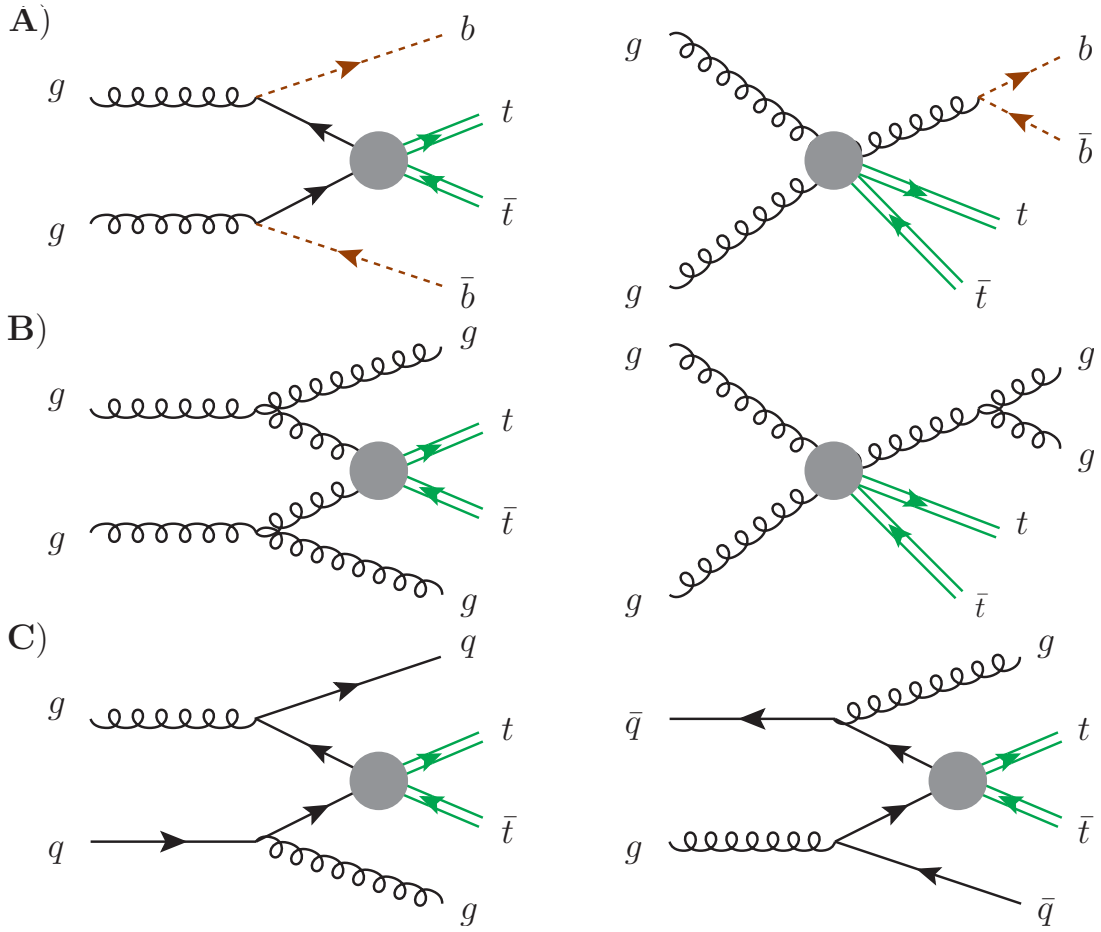

Figure 3. Feynman diagrams contributing to the dominant $gg \to t\bar{t}b\bar{b}$, $gg \to t\bar{t}gg$, $gq \to t\bar{t}gq$ and $g\bar{q} \to t\bar{t}g\bar{q}$ subprocesses for the following processes $pp \to t\bar{t}b\bar{b}$ and $pp \to t\bar{t}jj$ respectively. Blobs denote all possible substructures of the corresponding diagram.

All the next-to-leading order results presented in this paper have been obtained with the help of the package HELAC-NLO [51], which consists of HELAC-1LOOP [52–54] and HELAC-DIPOLES [55, 56]. The integration over the phase space has been achieved using KALEU [57].

To understand similarities and differences between the two backgrounds, it is helpful to identify the dominant partonic subprocesses. In the case of $pp \to t\bar{t}b\bar{b}$, at LO in the perturbative expansion, the most important production mechanism is via scattering of two gluons (see figure 3 - A). Within our selection cut choice, the gg channel contributes to the total LO cross section by about 90% at $\sqrt{s} = 8\,\text{TeV}$. On the other hand, $pp \to t\bar{t}jj$ is governed by two equally important channels, namely the gg channel (49%) and the qg/gq channel (40%) (see figure 3 - B and C). We note that the contribution of the process $gg \to t\bar{t}q\bar{q}$, which is related to the $t\bar{t}b\bar{b}$ final state amounts to 2.6% and is almost negligible compared to the dominant contributions. These facts suggest that the two backgrounds $t\bar{t}b\bar{b}$ and $t\bar{t}jj$ might show different features in the jet kinematics. This would have of course a negative impact on correlations.

JHEP07(2014)135

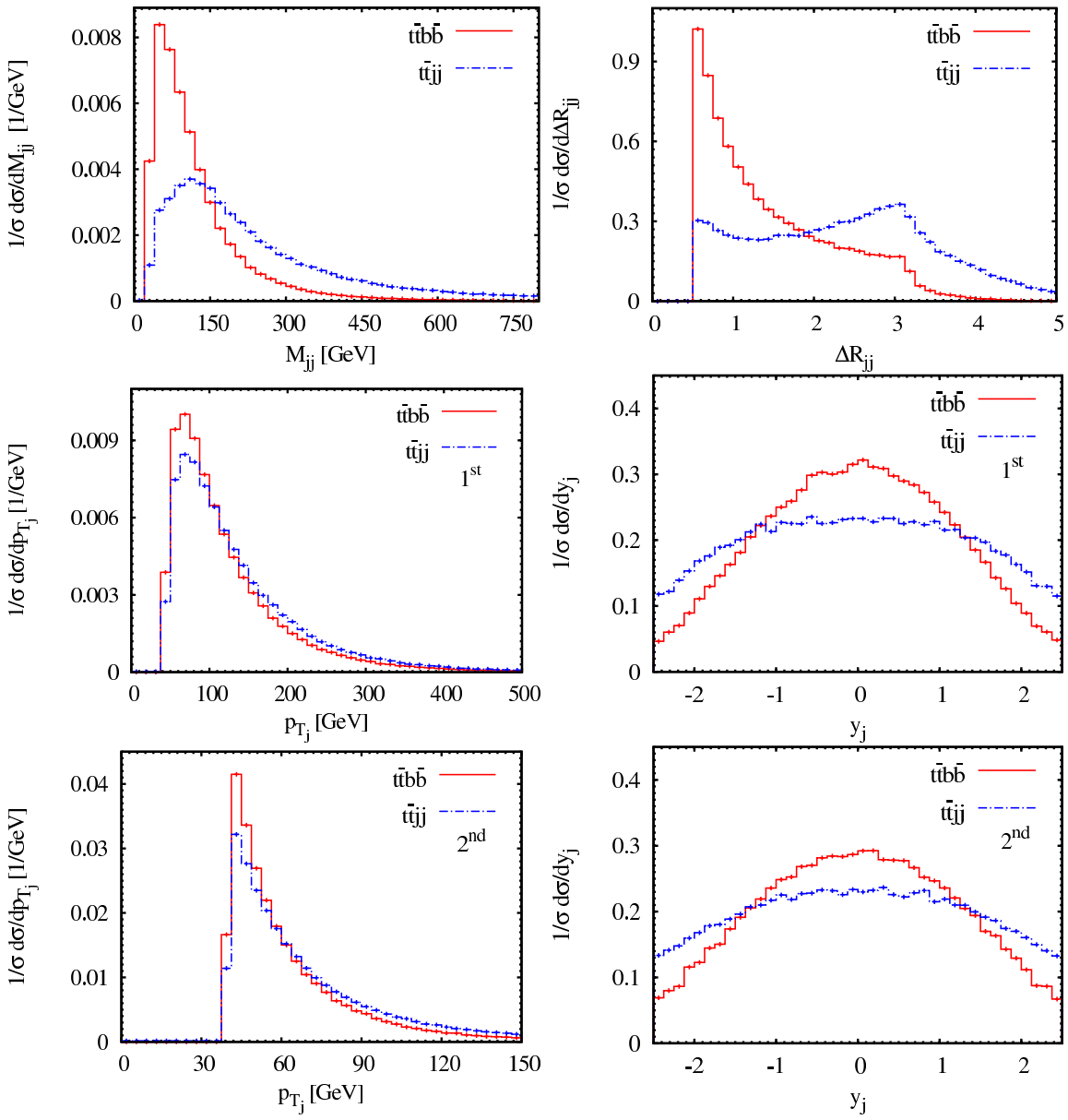

Figure 4. Comparison of the normalized next-to-leading order differential cross sections for $pp \to t\bar{t}b\bar{b}$ and $pp \to t\bar{t}jj$ at the LHC with $\sqrt{s} = 8\,\text{TeV}$. The dash-dotted (blue) curve corresponds to the $pp \to t\bar{t}jj$ process whereas the solid (red) curve to $pp \to t\bar{t}b\bar{b}$. The following distributions are shown: invariant mass of the two hardest jets, separation between those jets (upper panel), transverse momentum and rapidity of the first (middle panel) and the second hardest jet (lower panel).

JHEP07(2014)135

A collection of observables is reported in figure 4, where the NLO distributions have been normalized to the corresponding absolute cross sections, in order to evidentiate shape differences between the two processes. We focus here on quantities related to jet activity, such as rapidity and transverse momentum distributions of the first and the second hardest jet, invariant mass and separation between the two jets. Note that the requirement of two hard jets with a resolution parameter $R = 0.5$ and $p_{T_j}^{\min} = 40\,\text{GeV}$ implies a lower bound on their invariant mass, of the order of $m_{jj}^{\min} = 19.8\,\text{GeV}$.

We observe large shape differences in several observables, in line with our expectations. First of all, the b-jets show a preference for the central region of the detector in comparison with light jets. This difference is to be ascribed mainly to the contribution of the qg/gq channel, which favors the emission of jets at larger rapidities than the gg channel. Note that, contrary to the $t\bar{t}jj$ case, in $t\bar{t}b\bar{b}$ production the qg/gq channel is absent at LO and becomes available only at NLO.

In general, jets from the $t\bar{t}jj$ background show a much harder spectrum compared to $t\bar{t}b\bar{b}$. Sizeable differences can also be seen in the invariant mass and ΔR_{jj} separation between the two jets. In fact, using our cut selection, the $t\bar{t}b\bar{b}$ background is dominated by the $gg \to t\bar{t}g(g \to b\bar{b})$ production mechanism (see figure 3 - A.2), which naturally favors the production of b-jet pairs with small invariant mass. In the case of $t\bar{t}jj$, there is an interplay between two different mechanisms. On the one hand, $gg \to t\bar{t}g(g \to gg)$ (figure 3 - B.2) is relevant for small values of m_{jj} and gives a signature quite similar to the $b\bar{b}$ case. On the other hand, gluon radiation off initial-state partons (see *e.g* figure 3 - B.1) provides an equally important contribution due to collinear enhancements. Thus, light jets with large rapidities and large ΔR_{jj} separation are also likely to be produced in the $t\bar{t}jj$ case, which explains the quite different ΔR_{jj} spectrum. All the kinematical features described above are rather insensitive to higher-order corrections as shown in figure 5, where we compare normalized LO and NLO differential cross sections.

Despite sizeable differences in the jet activity, it might still be possible that $t\bar{t}b\bar{b}$ and $t\bar{t}jj$ show some similarity connected to the underlying basic process they have in common, *i.e.* top quark pair production. To this end, we report in figure 6 normalized distributions of a few observables related to the top quark kinematics, namely invariant mass of the $t\bar{t}$ system and averaged transverse momentum of top quarks. Indeed, distributions show a very good agreement in shape, indicating some level of correlation. The pretty different jet kinematics that characterizes the two backgrounds has a minimal influence on the underlying heavy $t\bar{t}$ system.

4 Next-to-leading order cross section ratio

In this section we present NLO predictions for the ratio $\sigma_{t\bar{t}b\bar{b}}/\sigma_{t\bar{t}jj}$ at the LHC for $\sqrt{s} =$ 7, 8 and 13 TeV. In addition to the basic selection cuts of eq. (2.4), we also report results for $R = 0.8$ and $\Delta R_{jj} > 0.8$ to check whether the impact of higher-order corrections is stable against these two parameters. Indeed we want to be confident that our choice $\Delta R_{jj}^{\min} = R = 0.5$ is well within the range of stability of the perturbative expansion.

JHEP07(2014)135

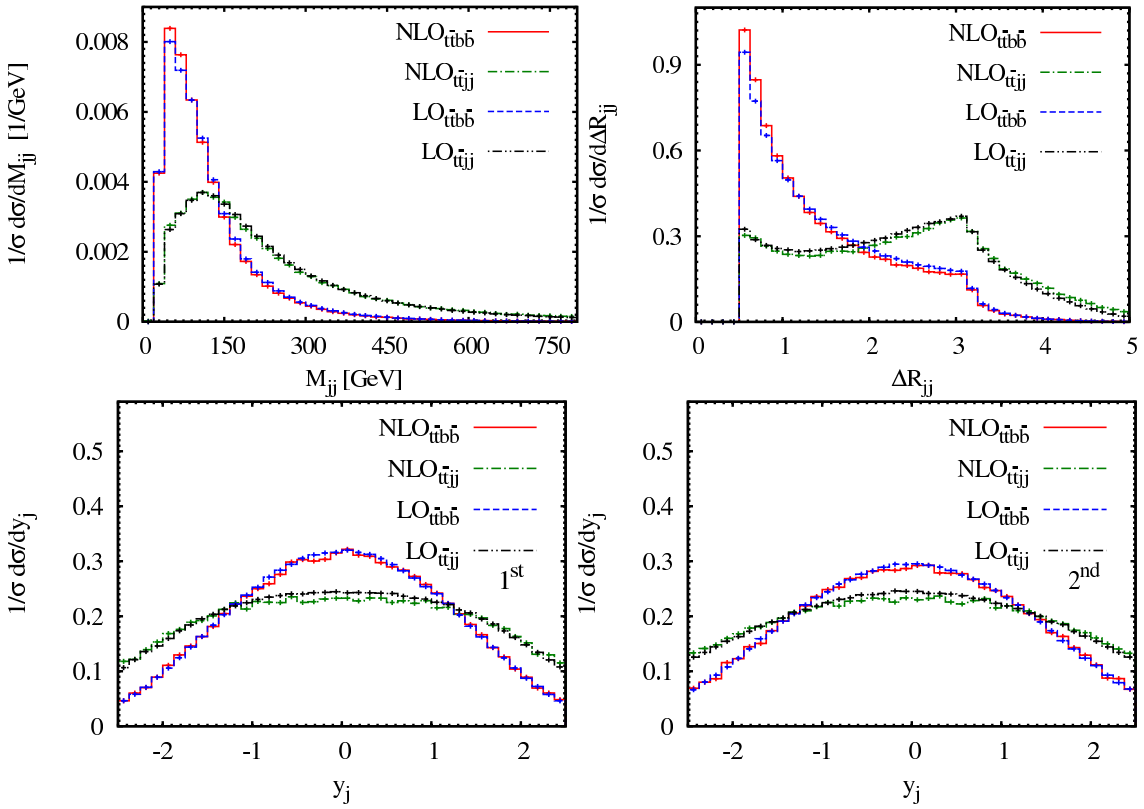

Figure 5. Comparison of the normalized leading order and next-to-leading order differential cross sections for $pp \to t\bar{t}b\bar{b}$ and $pp \to t\bar{t}jj$ at the LHC with $\sqrt{s} = 8\,\text{TeV}$. The following distributions are shown: invariant mass of the two hardest jets, separation between those jets and rapidity of the first and the second hardest jet.

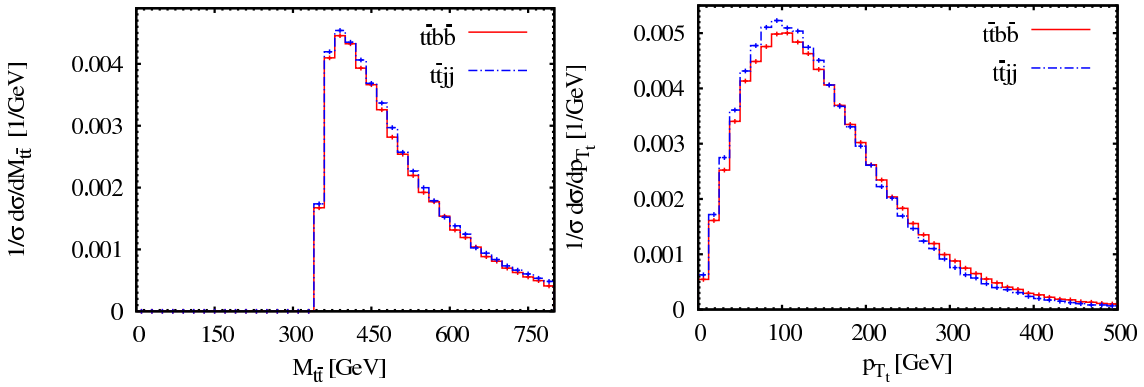

Figure 6. Comparison of the normalized next-to-leading order differential cross sections for $pp \to t\bar{t}b\bar{b}$ and $pp \to t\bar{t}jj$ at the LHC with $\sqrt{s} = 8\,\text{TeV}$. The dash-dotted (blue) curve corresponds to the $pp \to t\bar{t}jj$ process whereas the solid (red) curve to $pp \to t\bar{t}b\bar{b}$. The following distributions are shown: invariant mass of the $t\bar{t}$ system and (averaged) transverse momentum of the top quark.

JHEP07(2014)135

$\sqrt{s} = 7\,\text{TeV}$	$\sigma^{\text{NLO}}_{pp\to t\bar{t}b\bar{b}}$ [fb]	$\sigma^{\text{NLO}}_{pp\to t\bar{t}jj}$ [pb]	RATIO
$\Delta R_{jj} > 0.8,\ R = 0.8$	119.2 ± 0.1	13.66 ± 0.02	0.0087
$\Delta R_{jj} > 0.5,\ R = 0.5$	142.2 ± 0.2	13.55 ± 0.02	0.0105

Table 1. NLO cross sections for $pp \to t\bar{t}b\bar{b}$ and $pp \to t\bar{t}jj$ at the LHC with $\sqrt{s} = 7$ TeV, including errors from the Monte Carlo integration. The ratio $\sigma^{\text{NLO}}_{pp\to t\bar{t}b\bar{b}}/\sigma^{\text{NLO}}_{pp\to t\bar{t}jj}$ is also shown. Results for two different values of jet resolution parameter R and jets separation cut ΔR_{jj} are reported.

4.1 LHC @ 7 TeV

We start with the LHC results at $\sqrt{s} = 7\,\text{TeV}$. In table 1, absolute NLO cross sections are shown together with their ratio for two different values of the jet resolution parameter R and jet separation cut ΔR_{jj}. We observe that the cross section ratio is rather sensitive to the variation of those parameters. Decreasing ΔR_{jj} and R from 0.8 to 0.5 results in $+21\%$ change that is mostly due to a large, $+19\%$ shift in the NLO $t\bar{t}b\bar{b}$ cross section. The NLO $t\bar{t}jj$ cross section on the other hand is affected only by -1%. Since at the NLO jets may have some structure, i.e. two partons can be inside a jet, an interplay between two different effects can be observed. On the one hand, the simultaneous decrease of the ΔR_{jj} separation cut results in higher total NLO cross sections. On the other hand, a smaller resolution parameter R means that the probability of parton radiation outside the area with distance R is higher. This may be translated into a larger number of soft jets with $p_{T_j} < p^{\text{min}}_{T_j}$ and lower total NLO cross section. Since for the $t\bar{t}jj$ final state many events are concentrated around $\Delta R_{jj} = \pi$, the NLO cross section is mildly affected by a change in ΔR_{jj} cut from 0.8 to 0.5. Accordingly, the effect associated with the resolution parameter R dominates leading to the lower NLO cross section.

With $\Delta R_{jj} > 0.5$ and $R = 0.5$, i.e. for the values that have been used in the experimental studies [23], our predictions for the absolute cross sections read

$$\sigma^{\text{NLO}}_{t\bar{t}b\bar{b}}(\text{LHC}_{7\,\text{TeV}}, m_t = 173.5\ \text{GeV}, \text{CT10}) = 142.2^{+24.1(17\%)}_{-34.6(24\%)}\ [\text{fb}]\,, \tag{4.1}$$

and

$$\sigma^{\text{NLO}}_{t\bar{t}jj}(\text{LHC}_{7\,\text{TeV}}, m_t = 173.5\ \text{GeV}, \text{CT10}) = 13.55^{-1.66(14\%)}_{-1.92(14\%)}\ [\text{pb}]\,. \tag{4.2}$$

The theoretical uncertainty associated with neglected higher-order terms in the perturbative expansion, can be estimated by varying the renormalization and factorization scales up and down by a factor 2 around the central scale of the process, i.e. μ_0. The scale dependence is indicated by the upper/lower value, which corresponds to $0.5\mu_0/2\mu_0$. Our estimated scale uncertainties for the integrated cross sections are of the order $14\% - 24\%$ ($14\% - 20\%$ after symmetrisation). In addition, we find that the size of the NLO QCD corrections is moderately affected by lowering both ΔR_{jj} and R, i.e. changes of the order of

JHEP07(2014)135

15% or less are visible. Since those changes are within our theoretical errors, we conclude that $\Delta R_{jj}^{\min} = R = 0.5$ is still perturbatively valid and a fixed-order NLO calculation can be considered reliable.

We now turn to estimating the theoretical error for the cross section ratio. Given that there is no unique prescription for this in the literature, we decided to evaluate it using three different approaches. The first one assumes that the two background processes are not correlated, and consists in calculating all possible cross section ratios: $R = t\bar{t}b\bar{b}(\mu_1)/t\bar{t}jj(\mu_2)$, where $\mu_1, \mu_2 \in (0.5\mu_0, \mu_0, 2\mu_0)$. All possible combinations are considered, namely $(\mu_1, \mu_2) = \{(2,2), (2,1), (2,0.5), (0.5,2), (0.5,1), (0.5,0.5), (1,0.5)$ and $(1,2)\}$. The theoretical error band is determined taking the minimum and maximum values of the resulting ratios. This approach, that we name *uncorrelated*, gives the following result:

$$\sigma_{t\bar{t}b\bar{b}}^{\mathrm{NLO}}/\sigma_{t\bar{t}jj}^{\mathrm{NLO}}(\text{uncorrelated}) = 0.0105^{+0.0038(36\%)}_{-0.0026(25\%)}\,. \tag{4.3}$$

After symmetrisation of the error estimate, we get a scale uncertainty of 30% for the cross section ratio.

The second approach assumes that some degree of correlation exists, so the possible combinations to be evaluated are restricted to the subset $(\mu_1, \mu_2) = \{(2,2)$, and $(0.5,0.5)\}$. If $t\bar{t}b\bar{b}$ and $t\bar{t}jj$ are indeed correlated, a reduction of the scale uncertainty in the ratio should be expected. Using this approach, named *correlated*, we get the following result:

$$\sigma_{t\bar{t}b\bar{b}}^{\mathrm{NLO}}/\sigma_{t\bar{t}jj}^{\mathrm{NLO}}(\text{correlated}) = 0.0105^{+0.0034(32\%)}_{-0.0013(12\%)}\,. \tag{4.4}$$

Only a minor reduction in the size of the scale uncertainty is observed. The theoretical error band for the ratio is now 22% and is of the same order as the error for the absolute cross sections.

The third and last approach uses the relative errors of the absolute cross sections as input. We assume these quantities as uncorrelated and add the errors in quadrature, separately for the cases $0.5\mu_0$ and $2\mu_0$. This approach, that we name *relative error*, gives the result

$$\sigma_{t\bar{t}b\bar{b}}^{\mathrm{NLO}}/\sigma_{t\bar{t}jj}^{\mathrm{NLO}}(\text{relative error}) = 0.0105^{+0.0022(21\%)}_{-0.0029(28\%)}\,. \tag{4.5}$$

After symmetrisation of the error estimate, the final scale uncertainty is 24%.

4.2 LHC @ 8 TeV

We repeat the same procedure for the case $\sqrt{s} = 8\,\mathrm{TeV}$. The NLO cross sections are reported in table 2, together with the cross section ratio for the two different jet separation cuts and jet resolution parameters. Our conclusions are similar to the case of $\sqrt{s} = 7\,\mathrm{TeV}$ and therefore will be briefly summarized here. The absolute cross sections and corresponding theoretical errors for $\Delta R_{jj}^{\min} = R = 0.5$ are:

$$\sigma_{t\bar{t}b\bar{b}}^{\mathrm{NLO}}(\mathrm{LHC}_{8\,\mathrm{TeV}}, m_t = 173.5\ \mathrm{GeV}, \mathrm{CT10}) = 229.3^{+40.7(18\%)}_{-55.7(24\%)}\ [\mathrm{fb}]\,, \tag{4.6}$$

$$\sigma_{t\bar{t}jj}^{\mathrm{NLO}}(\mathrm{LHC}_{8\,\mathrm{TeV}}, m_t = 173.5\ \mathrm{GeV}, \mathrm{CT10}) = 20.97^{-3.25(15\%)}_{-2.79(13\%)}\ [\mathrm{pb}]\,. \tag{4.7}$$

JHEP07(2014)135

$\sqrt{s} = 8\,\text{TeV}$	$\sigma^{\text{NLO}}_{pp\to t\bar{t}b\bar{b}}$ [fb]	$\sigma^{\text{NLO}}_{pp\to t\bar{t}jj}$ [pb]	RATIO
$\Delta R_{jj} > 0.8,\ R = 0.8$	190.7 ± 0.2	21.15 ± 0.02	0.0090
$\Delta R_{jj} > 0.5,\ R = 0.5$	229.3 ± 0.3	20.97 ± 0.03	0.0109

Table 2. NLO cross sections for $pp \to t\bar{t}b\bar{b}$ and $pp \to t\bar{t}jj$ at the LHC with $\sqrt{s} = 8$ TeV, including errors from the Monte Carlo integration. The ratio $\sigma^{\text{NLO}}_{pp\to t\bar{t}b\bar{b}}/\sigma^{\text{NLO}}_{pp\to t\bar{t}jj}$ is also shown. Results for two different values of jet resolution parameter R and jets separation cut ΔR_{jj} are reported.

Accordingly, results for the cross section ratio are presented, and scale uncertainties evaluated according to the three methods described in the previous subsection:

$$\sigma^{\text{NLO}}_{t\bar{t}b\bar{b}}/\sigma^{\text{NLO}}_{t\bar{t}jj}(\text{uncorrelated}) = 0.0109^{+0.0043(39\%)}_{-0.0026(24\%)}\,,$$

$$\sigma^{\text{NLO}}_{t\bar{t}b\bar{b}}/\sigma^{\text{NLO}}_{t\bar{t}jj}(\text{correlated}) = 0.0109^{+0.0043(39\%)}_{-0.0014(13\%)}\,,$$

$$\sigma^{\text{NLO}}_{t\bar{t}b\bar{b}}/\sigma^{\text{NLO}}_{t\bar{t}jj}(\text{relative error}) = 0.0109^{+0.0026(24\%)}_{-0.0030(27\%)}\,. \tag{4.8}$$

After symmetrisation, the final theoretical errors amount to 32% for the uncorrelated case and 26% for the correlated one. Using the relative error approach, we find 26%. Scale uncertainties for the absolute $t\bar{t}b\bar{b}$ and $t\bar{t}jj$ cross sections are of the order of $15\% - 24\%$ ($14\% - 21\%$ after symmetrisation) and therefore comparable with the uncertainty of the ratio.

4.3 LHC @ 13 TeV

The case of $\sqrt{s} = 13\,\text{TeV}$ shows a similar pattern. The NLO cross sections for $t\bar{t}b\bar{b}$ and $t\bar{t}jj$ are reported in table 3, again for two different values of the jet resolution parameter R and jet separation cut ΔR_{jj}. For $\Delta R^{\text{min}}_{jj} = R = 0.5$ we find

$$\sigma^{\text{NLO}}_{t\bar{t}b\bar{b}}(\text{LHC}_{13\,\text{TeV}}, m_t = 173.5\ \text{GeV}, \text{CT10}) = 1078.3^{+222.1(20\%)}_{-249.7(23\%)}\ [\text{fb}]\,, \tag{4.9}$$

$$\sigma^{\text{NLO}}_{t\bar{t}jj}(\text{LHC}_{13\,\text{TeV}}, m_t = 173.5\ \text{GeV}, \text{CT10}) = 85.5^{-18.3(21\%)}_{-8.4(10\%)}\ [\text{pb}]\,. \tag{4.10}$$

Scale uncertainties of the integrated cross sections are at the same level as for $\sqrt{s} = 7$ and 8 TeV and amount to $21\% - 23\%$ ($16\% - 22\%$ after symmetrisation). The cross section ratio and its estimated error amount to

$$\sigma^{\text{NLO}}_{t\bar{t}b\bar{b}}/\sigma^{\text{NLO}}_{t\bar{t}jj}(\text{uncorrelated}) = 0.0126^{+0.0067(53\%)}_{-0.0029(23\%)}\,,$$

$$\sigma^{\text{NLO}}_{t\bar{t}b\bar{b}}/\sigma^{\text{NLO}}_{t\bar{t}jj}(\text{correlated}) = 0.0126^{+0.0067(53\%)}_{-0.0019(15\%)}\,,$$

$$\sigma^{\text{NLO}}_{t\bar{t}b\bar{b}}/\sigma^{\text{NLO}}_{t\bar{t}jj}(\text{relative error}) = 0.0126^{+0.0037(29\%)}_{-0.0032(25\%)}\,. \tag{4.11}$$

JHEP07(2014)135

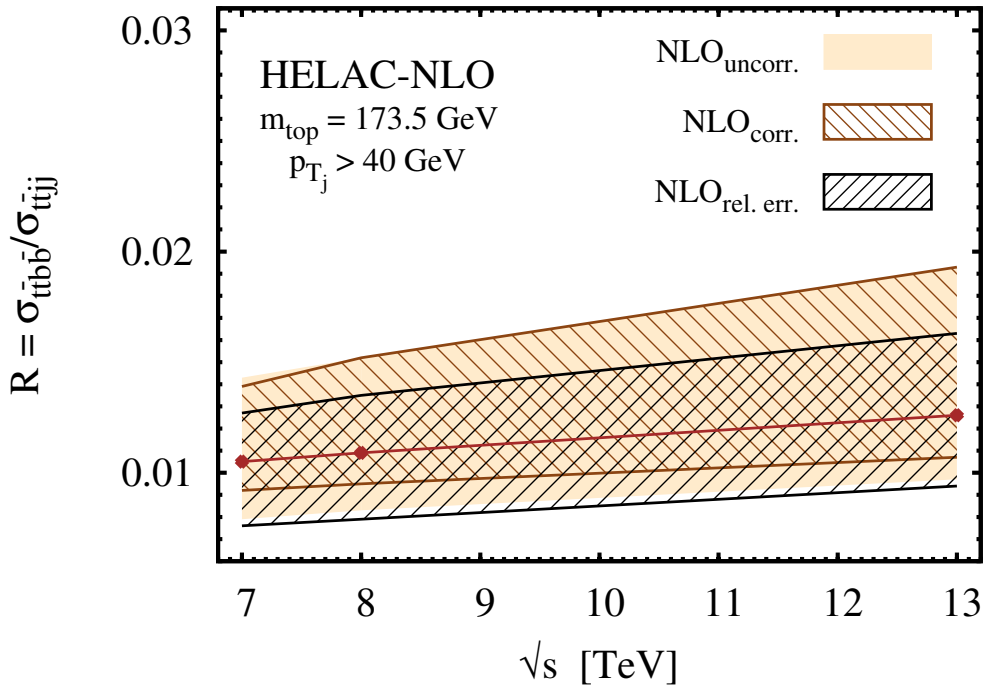

Figure 7. Theoretical prediction for the $\sigma_{t\bar{t}b\bar{b}}/\sigma_{t\bar{t}jj}$ ratio at the LHC as a function of the collider center-of-mass energy. Three uncertainty bands correspond to different methods of estimating scale variations.

For the uncorrelated case the theoretical error is 38%, whereas the correlated approach gives 34% and the relative-error approach 27%. We observe here that the cross section ratio and its uncertainty increases with the center-of-mass energy and the difference between uncertainties evaluated in the correlated and uncorrelated approaches becomes smaller. The theoretical error on the ratio is in this case slightly larger than the corresponding one on the absolute cross sections.

We summarize our predictions in figure 7, where the cross section ratio is presented as a function of the collider center-of-mass energy. The plot shows three different error bands according to the three methods employed for the uncertainty estimation. The error bands are relatively independent on the method adopted. The *uncorrelated* approach being the most conservative one. We decided to adopt the latter for our comparison with the LHC data at $\sqrt{s} = 8\,\text{TeV}$, that will be discussed in the next section.

5 Comparison with CMS results at $\sqrt{s} = 8$ TeV

We now compare our NLO predictions with the corresponding measurement of the ratio $\sigma_{t\bar{t}b\bar{b}}/\sigma_{t\bar{t}jj}$ by the CMS Collaboration [23, 58], based on a data sample corresponding to an integrated luminosity of 19.6 fb^{-1} collected at $\sqrt{s} = 8\,\text{TeV}$ in the di-lepton decay mode. We quote below the experimental result, which has been derived from the inclusive $t\bar{t}b\bar{b}$ and

JHEP07(2014)135

$\sqrt{s} = 13\,\text{TeV}$	$\sigma^{\text{NLO}}_{pp\to t\bar{t}b\bar{b}}$ [fb]	$\sigma^{\text{NLO}}_{pp\to t\bar{t}jj}$ [pb]	RATIO
$\Delta R_{jj} > 0.8,\ R = 0.8$	886.8 ± 1.4	86.7 ± 0.1	0.0102
$\Delta R_{jj} > 0.5,\ R = 0.5$	1078.3 ± 1.2	85.5 ± 0.2	0.0126

Table 3. NLO cross sections for $pp \to t\bar{t}b\bar{b}$ and $pp \to t\bar{t}jj$ at the LHC with $\sqrt{s} = 13$ TeV, including errors from the Monte Carlo integration. The ratio $\sigma^{\text{NLO}}_{pp\to t\bar{t}b\bar{b}}/\sigma^{\text{NLO}}_{pp\to t\bar{t}jj}$ is also shown. Results for two different values of jet resolution parameter R and jets separation cut ΔR_{jj} are reported.

$t\bar{t}jj$ cross sections already unfolded to the full phase space for the top quark. In addition, the $t\bar{t}jj$ sample contains contributions from light-, charm- and bottom-jets. Both rates take also into account the branching ratio of the di-lepton decay mode of 10.8% [39] and corrections to the parton level jets. The result has been obtained for jets that are required to carry $p_{T_j} > 20\,\text{GeV}$ ($p_{T_j} > 40\,\text{GeV}$), to be located in the rapidity range of $|y_j| < 2.5$ and to be separated in the rapidity-azimuthal angle plane by $\Delta R_{jj} > 0.5$:

$$\sigma_{t\bar{t}b\bar{b}}/\sigma_{t\bar{t}jj}(\text{LHC}_{8\,\text{TeV}}, p_{T_j} > 20\ \text{GeV}) = 0.021 \pm 0.003\ (\text{stat.}) \pm 0.005\ (\text{syst.})\,, \quad (5.1)$$

$$\sigma_{t\bar{t}b\bar{b}}/\sigma_{t\bar{t}jj}(\text{LHC}_{8\,\text{TeV}}, p_{T_j} > 40\ \text{GeV}) = 0.022 \pm 0.005\ (\text{stat.}) \pm 0.005\ (\text{syst.})\,. \quad (5.2)$$

A total systematic uncertainty of 22.6% has been estimated by CMS, where the dominant contribution for $p_{T_j} > 40\,\text{GeV}$ comes from the mistag rate (12.6%) and the b-jet tagging efficiency (11.2%) [23]. Several experimental systematic uncertainties are reduced by taking the cross section ratio, as expected.

We can directly compare the measured ratio for $p_{T_j} > 40\,\text{GeV}$ with the corresponding HELAC-NLO prediction at $\sqrt{s} = 8\,\text{TeV}$:

$$\sigma^{\text{NLO}}_{t\bar{t}b\bar{b}}/\sigma^{\text{NLO}}_{t\bar{t}jj}(\text{LHC}_{8\,\text{TeV}}, m_t = 173.5\ \text{GeV}, \text{CT10}) = 0.0109 + 0.0043 - 0.0026\,. \quad (5.3)$$

Let us remind that we have adopted here the most conservative *uncorrelated* approach for our theoretical error estimate. As figure 8 also shows, our prediction calculated for the central scale differs by a factor of 2 from the experimental number. However, with the present level of accuracy the two results agree within 1.4σ. To facilitate the comparison, systematic and statistical uncertainties reported by the CMS experiment have been taken as uncorrelated and thus added in quadrature. The total experimental error obtained in this way amounts at present to ± 0.0071 (32%).

Let us conclude this section by discussing the impact of the top quark decays on the $t\bar{t}b\bar{b}/t\bar{t}jj$ ratio. To this end, we compare ratios evaluated with undecayed and decayed top quarks at the LO. First we have evaluated the ratio for $p_{T_j} > 40\,\text{GeV}$, $|y_j| < 2.5$ and $\Delta R_{jj} > 0.5$ at the LHC with $\sqrt{s} = 8\,\text{TeV}$ using on-shell top quarks for both processes i.e. $\sigma^{\text{LO}}_{t\bar{t}b\bar{b}}$ and $\sigma^{\text{LO}}_{t\bar{t}jj}$ at $\mathcal{O}(\alpha_s^4)$. In the next step leptonic decays of W gauge bosons have been included. More specifically $pp \to e^+\nu_e\mu^-\bar{\nu}_\mu b\bar{b}b\bar{b}$ and $pp \to e^+\nu_e\mu^-\bar{\nu}_\mu b\bar{b}jj$ processes

JHEP07(2014)135

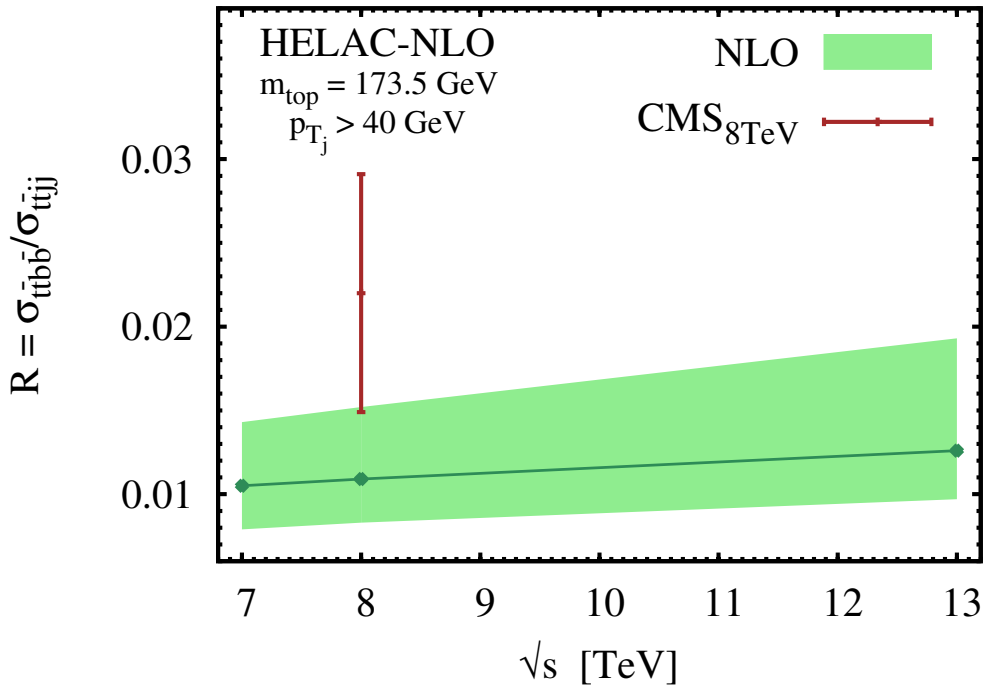

Figure 8. Theoretical prediction for the $\sigma_{t\bar{t}b\bar{b}}/\sigma_{t\bar{t}jj}$ ratio at the LHC as a function of the collider center-of-mass energy, compared to the available measurement result from CMS with $\sqrt{s} = 8\,\text{TeV}$. The uncertainty band depicts scale variation.

have been calculated with the help of HELAC-PHEGAS, where full off-shell and finite width top and W effects have been included by taking into account the double-resonant, single-resonant and non-resonant contributions at order $\mathcal{O}(\alpha_s^4\alpha^4)$. Example of Feynman diagrams contributing to the LO $pp \to t\bar{t}b\bar{b}$ and $pp \to e^+\nu_e\mu^-\bar{\nu}_\mu b\bar{b}b\bar{b}$ processes are presented in figure 9 and figure 10. The following basic selection has been applied to (anti-)top decay products to ensure that the leptons are observed inside the detector and are well separated from each other:

$$p_{T_\ell} > 20\ \text{GeV}, \quad |\eta_\ell| < 2.5, \quad \Delta R_{\ell\ell} > 0.4, \quad \Delta R_{\ell j} > 0.4, \quad p_T^{\text{miss}} > 30\ \text{GeV}\,, \tag{5.4}$$

where p_T^{miss} is the transverse momentum of the system of two neutrinos. The impact of the top quark decays on the $\sigma_{t\bar{t}b\bar{b}}/\sigma_{t\bar{t}jj}$ cross section ratio has been established to be less than 5%, well within the estimated dominant theoretical uncertainties.

6 Conclusions

In this paper we have presented the first consistent NLO theoretical predictions for the cross section ratio $\sigma_{ttbb}/\sigma_{ttjj}$ in order to help high-quality comparisons with the data collected at the LHC. We have considered the case of both present and future collider energies, $\sqrt{s} = 7$, 8 and 13 TeV, exploring different methods to provide as much realistic estimates

JHEP07(2014)135

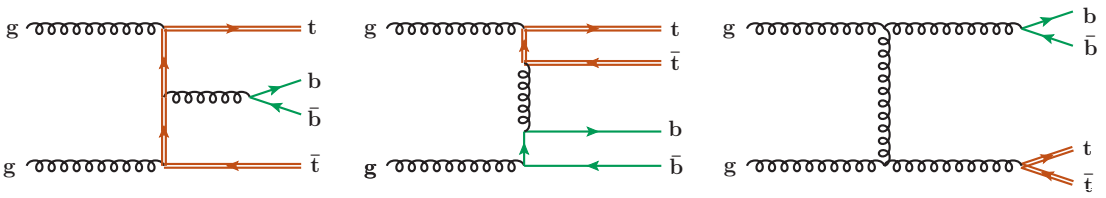

Figure 9. Example of Feynman diagrams contributing to the irreducible background $pp \to t\bar{t}b\bar{b}$ at $\mathcal{O}(\alpha_s^4)$.

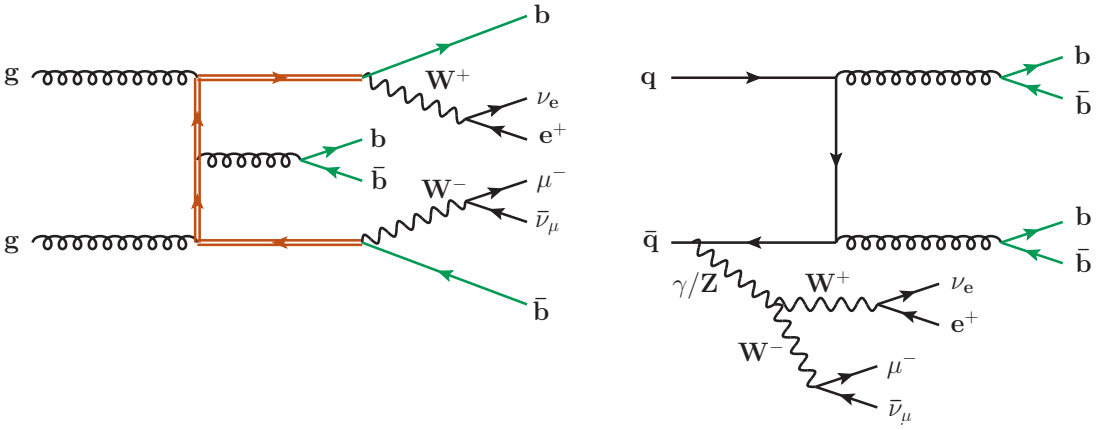

Figure 10. Example of Feynman diagrams contributing to the irreducible background $pp \to e^+\nu_e\mu^-\bar{\nu}_\mu b\bar{b}b\bar{b}$ at $\mathcal{O}(\alpha_s^4\alpha^4)$ with double-resonant (left panel) and non-resonant (right panel) top quark contributions.

as possible of the scale uncertainty for our predictions. We have found that our estimate is relatively independent on the method applied. The method which assumes $t\bar{t}b\bar{b}$ and $t\bar{t}jj$ uncorrelated should be taken as the most conservative one. Moreover, we have shown that the scale uncertainty of the ratio, at the level of $20\% - 30\%$, is comparable with the error on the absolute cross sections $\sigma(t\bar{t}b\bar{b})$ and $\sigma(t\bar{t}jj)$. Given that this uncertainty is the dominant theoretical error for the processes at hand, we conclude that the ratio shows the same theoretical accuracy as the individual cross sections.[3]

Let us remind that top quark decays are not included in our study. This corresponds to the unrealistic situation of a perfect top quark reconstruction with all decay channels included. Besides, the two light or b-jets are always assumed not to be misassociated with the top quark decay products. It is clearly desirable to include top quark decays and study how they affect the cross section ratio. However, we expect a moderate impact, provided the same method of reconstructing the $t\bar{t}$ system is used in both processes, because the top quarks show a rather similar kinematics dependence in $t\bar{t}b\bar{b}$ and $t\bar{t}jj$ backgrounds. This correlation might be helpful to better distinguish whether the reconstructed b-jets come from the $t\bar{t}$ pair, or e.g. from the QCD $g \to b\bar{b}$ splitting. This assumption is further

[3]We note, however, that ratios and double ratios of cross sections calculated at different center-of-mass energies could lead to predictions with higher precision [59].

JHEP07(2014)135

supported by the study we have performed at the LO where very moderate effects on the ratio coming from the top quark decays have been found.

The results presented in this paper have been obtained at the partonic level, and parton shower effects should, in principle, be included. We expect the parton shower to play an important role in case of loose cuts on jet p_T, i.e. for $p_{T_j} \ll 40\,\text{GeV}$, where a question mark is put on the reliability of a genuine fixed-order calculation. First results for $t\bar{t}$ production in association with up to two jets merged with parton shower have recently started to appear [31], but the assumed kinematical restriction on the jet p_T (40 GeV, 60 GeV or 80 GeV) seems still too high to shed light on such effects. We note that the estimated uncertainty on the absolute cross section for the production of the $t\bar{t}jj$ system presented there is comparable with our estimates. Similar conclusions apply as well to the case of $t\bar{t}b\bar{b}$ production, recently matched to the parton shower [32]. Scale variations before and after matching have been assessed to be rather similar, at the level of $20\% - 30\%$ which is again in agreement with our estimates. Given all these reasons, we believe that parton shower effects will have a minimal impact on our results in the considered kinematical range.

Finally, we have presented a comparison between our NLO predictions and the currently available CMS data for $\sqrt{s} = 8\,\text{TeV}$. The present level of agreement is not striking but still within the uncertainties. However, new measurements of the cross section ratio, based on the complete data samples collected by both the CMS and the ATLAS experiments, are underway. Those enlarged data samples, including other top quark decay channels, will provide more accurate measurements, which we are looking forward to compare with our predictions.

Acknowledgments

The authors would like to thank colleagues from the ATLAS and CMS experiments for motivating them to perform this study. We acknowledge Tae Jeong Kim for useful discussions, and Adam Kardos for clarifications concerning parameter settings in Pythia.

The work of M. Worek was supported in part by the DFG under Grant No. WO 1900/1-1 (*"Signals and Backgrounds Beyond Leading Order. Phenomenological studies for the LHC")* and by the Research Funding Program Aristeta, *"Higher Order Calculations and Tools for High Energy Colliders"*, HOCTools (co-financed by the European Union (European Social Fund ESF) and Greek national funds through the Operational Program *"Education and Lifelong Learning"* of the National Strategic Reference Framework (NSRF)).

References

[1] ATLAS collaboration, *Observation of a new particle in the search for the Standard Model Higgs boson with the ATLAS detector at the LHC*, *Phys. Lett.* **B 716** (2012) 1 [arXiv:1207.7214] [inSPIRE].

JHEP07(2014)135

[2] CMS collaboration, *Observation of a new boson at a mass of 125 GeV with the CMS experiment at the LHC*, *Phys. Lett.* **B 716** (2012) 30 [arXiv:1207.7235] [INSPIRE].

[3] A. Djouadi, *The Anatomy of electro-weak symmetry breaking. I: The Higgs boson in the standard model*, *Phys. Rept.* **457** (2008) 1 [hep-ph/0503172] [INSPIRE].

[4] ATLAS collaboration, *Search for the Standard Model Higgs boson produced in association with a vector boson and decaying to a b-quark pair with the ATLAS detector*, *Phys. Lett.* **B 718** (2012) 369 [arXiv:1207.0210] [INSPIRE].

[5] CMS collaboration, *Search for the standard model Higgs boson decaying to bottom quarks in pp collisions at* $\sqrt{s} = 7$ *TeV*, *Phys. Lett.* **B 710** (2012) 284 [arXiv:1202.4195] [INSPIRE].

[6] CMS collaboration, *Search for the standard model Higgs boson produced in association with a top-quark pair in pp collisions at the LHC*, *JHEP* **05** (2013) 145 [arXiv:1303.0763] [INSPIRE].

[7] CMS collaboration, *Search for the standard model Higgs boson produced in association with a W or a Z boson and decaying to bottom quarks*, *Phys. Rev.* **D 89** (2014) 012003 [arXiv:1310.3687] [INSPIRE].

[8] K. Desch and M. Schumacher, *Model independent determination of the top Yukawa coupling from LHC and LC*, *Eur. Phys. J.* **C 46** (2006) 527 [hep-ph/0407159] [INSPIRE].

[9] R. Lafaye, T. Plehn, M. Rauch, D. Zerwas and M. Dührssen, *Measuring the Higgs Sector*, *JHEP* **08** (2009) 009 [arXiv:0904.3866] [INSPIRE].

[10] M. Klute, R. Lafaye, T. Plehn, M. Rauch and D. Zerwas, *Measuring Higgs Couplings from LHC Data*, *Phys. Rev. Lett.* **109** (2012) 101801 [arXiv:1205.2699] [INSPIRE].

[11] F. Caola and K. Melnikov, *Constraining the Higgs boson width with ZZ production at the LHC*, *Phys. Rev.* **D 88** (2013) 054024 [arXiv:1307.4935] [INSPIRE].

[12] J.M. Campbell, R.K. Ellis and C. Williams, *Bounding the Higgs width at the LHC using full analytic results for* $gg \to e^-e^+\mu^-\mu^+$, *JHEP* **04** (2014) 060 [arXiv:1311.3589] [INSPIRE].

[13] J.M. Campbell, R.K. Ellis and C. Williams, *Bounding the Higgs width at the LHC: complementary results from* $H \to WW$, *Phys. Rev.* **D 89** (2014) 053011 [arXiv:1312.1628] [INSPIRE].

[14] CMS Collaboration, *Constraints on the Higgs boson width from off-shell production and decay to* $ZZ \to \ell\ell\ell'\ell'$ *and* $\ell\ell\nu\nu$, CMS-PAS-HIG-14-0202.

[15] V. Drollinger, T. Müller and D. Denegri, *Searching for Higgs bosons in association with top quark pairs in the* $H_0 \to b\bar{b}$ *decay mode*, hep-ph/0111312 [INSPIRE].

[16] ATLAS collaboration, *Search for the Standard Model Higgs boson produced in association with top quarks in proton-proton collisions at* $\sqrt{s} = 7$ *TeV using the ATLAS detector*, ATLAS-CONF-2012-135.

[17] CMS Collaboration, *Search for Higgs boson production in association with top quark pairs in pp collisions*, CMS-PAS-HIG-12-025.

[18] CMS Collaboration, *Search for Higgs Boson Production in Association with a Top-Quark Pair and Decaying to Bottom Quarks or Tau Leptons*, CMS-PAS-HIG-13-019.

[19] T. Plehn, G.P. Salam and M. Spannowsky, *Fat Jets for a Light Higgs*, *Phys. Rev. Lett.* **104** (2010) 111801 [arXiv:0910.5472] [INSPIRE].

JHEP07(2014)135

[20] P. Artoisenet, P. de Aquino, F. Maltoni and O. Mattelaer, *Unravelling $t\bar{t}h$ via the Matrix Element Method*, *Phys. Rev. Lett.* **111** (2013) 091802 [arXiv:1304.6414] [INSPIRE].

[21] J. Bramante, A. Delgado and A. Martin, *Cornering a Hyper Higgs: Angular Kinematics for Boosted Higgs Bosons with Top Pairs*, *Phys. Rev.* **D 89** (2014) 093006 [arXiv:1402.5985] [INSPIRE].

[22] CMS Collaboration, *First Measurement of the cross section ratio ttbb/ttjj in pp Collisions at* $\sqrt{s}$, CMS-PAS-TOP-12-024.

[23] CMS Collaboration, *Measurement of the cross section ratio ttbb/ttjj in pp Collisions at 8 TeV*, CMS-PAS-TOP-13-010.

[24] ATLAS collaboration, *A study of heavy flavor quarks produced in association with top quark pairs at* $\sqrt{s} = 7$ *TeV using the ATLAS detector*, *Phys. Rev.* **D 89** (2014) 072012 [arXiv:1304.6386] [INSPIRE].

[25] A. Bredenstein, A. Denner, S. Dittmaier and S. Pozzorini, *NLO QCD corrections to* $pp \to t\bar{t}b\bar{b} + X$ *at the LHC*, *Phys. Rev. Lett.* **103** (2009) 012002 [arXiv:0905.0110] [INSPIRE].

[26] G. Bevilacqua, M. Czakon, C.G. Papadopoulos, R. Pittau and M. Worek, *Assault on the NLO Wishlist:* $pp \to t\bar{t}b\bar{b}$, *JHEP* **09** (2009) 109 [arXiv:0907.4723] [INSPIRE].

[27] A. Bredenstein, A. Denner, S. Dittmaier and S. Pozzorini, *NLO QCD Corrections to Top Anti-Top Bottom Anti-Bottom Production at the LHC: 2. full hadronic results*, *JHEP* **03** (2010) 021 [arXiv:1001.4006] [INSPIRE].

[28] M. Worek, *On the next-to-leading order QCD K-factor for top $t\bar{t}b\bar{b}$ production at the Tevatron*, *JHEP* **02** (2012) 043 [arXiv:1112.4325] [INSPIRE].

[29] G. Bevilacqua, M. Czakon, C.G. Papadopoulos and M. Worek, *Dominant QCD Backgrounds in Higgs Boson Analyses at the LHC: A Study of* $pp \to t\bar{t}$ *+ 2 jets at Next-To-Leading Order*, *Phys. Rev. Lett.* **104** (2010) 162002 [arXiv:1002.4009] [INSPIRE].

[30] G. Bevilacqua, M. Czakon, C.G. Papadopoulos and M. Worek, *Hadronic top-quark pair production in association with two jets at Next-to-Leading Order QCD*, *Phys. Rev.* **D 84** (2011) 114017 [arXiv:1108.2851] [INSPIRE].

[31] S. Hoeche, F. Krauss, P. Maierhoefer, S. Pozzorini, M. Schonherr et al., *Next-to-leading order QCD predictions for top-quark pair production with up to two jets merged with a parton shower*, arXiv:1402.6293 [INSPIRE].

[32] F. Cascioli, P. Maierhoefer, N. Moretti, S. Pozzorini and F. Siegert, *NLO matching for ttbb production with massive b-quarks*, arXiv:1309.5912 [INSPIRE].

[33] A. Kardos and Z. Trócsányi, *Hadroproduction of $t\bar{t}$ pair with a $b\bar{b}$ pair using PowHel*, *J. Phys.* **G 41** (2014) 075005 [arXiv:1303.6291] [INSPIRE].

[34] A. Kanaki and C.G. Papadopoulos, *HELAC: A Package to compute electroweak helicity amplitudes*, *Comput. Phys. Commun.* **132** (2000) 306 [hep-ph/0002082] [INSPIRE].

[35] C.G. Papadopoulos, *PHEGAS: A Phase space generator for automatic cross-section computation*, *Comput. Phys. Commun.* **137** (2001) 247 [hep-ph/0007335] [INSPIRE].

[36] A. Cafarella, C.G. Papadopoulos and M. Worek, *Helac-Phegas: A Generator for all parton level processes*, *Comput. Phys. Commun.* **180** (2009) 1941 [arXiv:0710.2427] [INSPIRE].

JHEP07(2014)135

[37] J. Alwall, A. Ballestrero, P. Bartalini, S. Belov, E. Boos et al., *A Standard format for Les Houches event files*, *Comput. Phys. Commun.* **176** (2007) 300 [hep-ph/0609017] [INSPIRE].

[38] T. Sjöstrand, S. Mrenna and P.Z. Skands, *PYTHIA 6.4 Physics and Manual*, *JHEP* **05** (2006) 026 [hep-ph/0603175] [INSPIRE].

[39] Particle Data Group collaboration, J. Beringer et al., *Review of Particle Physics (RPP)*, *Phys. Rev.* **D 86** (2012) 010001 [INSPIRE].

[40] W. Giele, E.W.N. Glover, I. Hinchliffe, J. Huston, E. Laenen et al., *The QCD/SM working group: Summary report*, hep-ph/0204316 [INSPIRE].

[41] M.R. Whalley, D. Bourilkov and R.C. Group, *The Les Houches accord PDFs (LHAPDF) and LHAGLUE*, hep-ph/0508110 [INSPIRE].

[42] D. Bourilkov, R.C. Group and M.R. Whalley, *LHAPDF: PDF use from the Tevatron to the LHC*, hep-ph/0605240 [INSPIRE].

[43] H.-L. Lai, J. Huston, S. Mrenna, P. Nadolsky, D. Stump et al., *Parton Distributions for Event Generators*, *JHEP* **04** (2010) 035 [arXiv:0910.4183] [INSPIRE].

[44] M. Cacciari, G.P. Salam and G. Soyez, *The Anti-k(t) jet clustering algorithm*, *JHEP* **04** (2008) 063 [arXiv:0802.1189] [INSPIRE].

[45] M. Cacciari, G.P. Salam and G. Soyez, *FastJet User Manual*, *Eur. Phys. J.* **C 72** (2012) 1896 [arXiv:1111.6097] [INSPIRE].

[46] M. Cacciari and G.P. Salam, *Dispelling the N^3 myth for the k_t jet-finder*, *Phys. Lett.* **B 641** (2006) 57 [hep-ph/0512210] [INSPIRE].

[47] M.L. Mangano, M. Moretti, F. Piccinini and M. Treccani, *Matching matrix elements and shower evolution for top-quark production in hadronic collisions*, *JHEP* **01** (2007) 013 [hep-ph/0611129] [INSPIRE].

[48] S. Alioli, S.-O. Moch and P. Uwer, *Hadronic top-quark pair-production with one jet and parton showering*, *JHEP* **01** (2012) 137 [arXiv:1110.5251] [INSPIRE].

[49] CMS collaboration, *Identification of b-quark jets with the CMS experiment*, 2013 *JINST* **8** P04013 [arXiv:1211.4462] [INSPIRE].

[50] H.-L. Lai, M. Guzzi, J. Huston, Z. Li, P.M. Nadolsky et al., *New parton distributions for collider physics*, *Phys. Rev.* **D 82** (2010) 074024 [arXiv:1007.2241] [INSPIRE].

[51] G. Bevilacqua, M. Czakon, M.V. Garzelli, A. van Hameren, A. Kardos et al., *HELAC-NLO*, *Comput. Phys. Commun.* **184** (2013) 986 [arXiv:1110.1499] [INSPIRE].

[52] A. van Hameren, C.G. Papadopoulos and R. Pittau, *Automated one-loop calculations: A Proof of concept*, *JHEP* **09** (2009) 106 [arXiv:0903.4665] [INSPIRE].

[53] G. Ossola, C.G. Papadopoulos and R. Pittau, *CutTools: A Program implementing the OPP reduction method to compute one-loop amplitudes*, *JHEP* **03** (2008) 042 [arXiv:0711.3596] [INSPIRE].

[54] A. van Hameren, *OneLOop: For the evaluation of one-loop scalar functions*, *Comput. Phys. Commun.* **182** (2011) 2427 [arXiv:1007.4716] [INSPIRE].

[55] M. Czakon, C.G. Papadopoulos and M. Worek, *Polarizing the Dipoles*, *JHEP* **08** (2009) 085 [arXiv:0905.0883] [INSPIRE].

JHEP07(2014)135

[56] G. Bevilacqua, M. Czakon, M. Kubocz and M. Worek, *Complete Nagy-Soper subtraction for next-to-leading order calculations in QCD*, *JHEP* **10** (2013) 204 [arXiv:1308.5605] [INSPIRE].

[57] A. van Hameren, *Kaleu: A General-Purpose Parton-Level Phase Space Generator*, arXiv:1003.4953 [INSPIRE].

[58] CMS Collaboration, *Measurement of Top-quark Pair Production in Association with a b-quark Pair in pp Collisions at* $\sqrt{s} = 8$ *TeV in Final States with Two Leptons*, in preparation.

[59] M.L. Mangano and J. Rojo, *Cross Section Ratios between different CM energies at the LHC: opportunities for precision measurements and BSM sensitivity*, *JHEP* **08** (2012) 010 [arXiv:1206.3557] [INSPIRE].

JHEP07(2014)135